ACS OMEGA

Article

Cite This: ACS Omega 2019, 4, 7411−7419

http://pubs.acs.org/journal/acsodf

Controlled Growth of the Noncentrosymmetric $Zn(3\text{-ptz})_2$ and Zn(OH)(3-ptz) Metal−Organic Frameworks

Javier Enríquez,[†,‡] Carolina Manquian,[†,‡] Ignacio Chi-Duran,[‡,§] Felipe Herrera,*[,‡,§] and Dinesh Pratap Singh*[,‡,§]

[†]Department of Metallurgical Engineering, Faculty of Engineering, University of Santiago Chile, Av. Lib. Bernardo O'Higgins 3363, Estación Central, 9170022 Santiago, Chile

[‡]Department of Physics, Faculty of Science, University of Santiago Chile, Avenida Ecuador 3493, Estación Central, 9170124 Santiago, Chile

[§]Millennium Institute for Research in Optics (MIRO), Av. Esteban Iturra S/N, Concepción, 4030000 Concepción, Chile

Supporting Information

ABSTRACT: Noncentrosymmetric single-crystal metal−organic frameworks (MOFs) are promising candidates for phase-matched nonlinear optical communication. However, the typical hydrothermal synthesis conditions produce small crystals with relatively low transmittance and poor phase matching. In the search for optimal crystal morphology, we study the effect of the metal-to-ligand molar ratio and reaction pH on the hydrothermal synthesis of the noncentrosymmetric **$Zn(3\text{-ptz})_2$** and **Zn(OH)(3-ptz)** MOFs with in situ ligand formation. In acidic environments, we find that decreasing the amount of ligand below the stoichiometric molar ratio 1:2 also produces highly transparent single-crystal octahedrons of **$Zn(3\text{-ptz})_2$**. In alkaline environments, we obtain long rodlike **Zn(OH)(3-ptz)** crystals whose length exceeds previous reports by up to 4 orders of magnitude. All reaction products are characterized by using powder X-ray diffraction, Fourier transform infrared spectroscopy, optical and scanning electron microscopy, and solid-state UV−visible spectroscopy. Additionally, we find an alternative synthesis route for the recently reported high-energy MOF **$Zn(3\text{-ptz})N_3$**. Potential applications of these results in the development of MOF-based nonlinear optical devices are discussed.

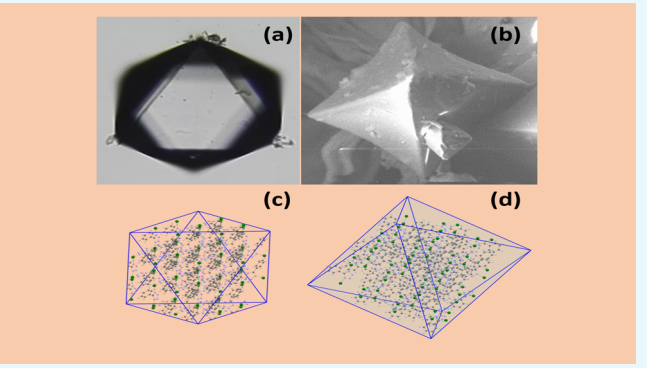

INTRODUCTION

Functional crystalline materials based on metal−organic frameworks (MOFs) have been intensely studied over the past decade because of the diverse set of applications enabled by properties such as ultrahigh porosity,[1−6] record high pore aperture size,[5,7] high thermal and chemical stability,[8−13] and nonlinear optical activity.[14−23] MOF materials have been successfully used for applications in gas storage and separation,[24−27] fuel cells,[28−31] chemical sensing,[32−34] biomedical imaging,[35−37] and drug delivery.[38,39] Several methods can be used to synthesize MOFs including microwave-assisted synthesis,[40,41] slow evaporation synthesis,[42,43] sonochemical synthesis,[44,45] mechanochemical synthesis,[46,47] electrochemical synthesis,[48,49] and hydro-/solvothermal synthesis.[50,51] Different synthesis methods produce structures with characteristic size, homogeneity, and morphology, which are directly related with the performance of the grown MOF crystals in applications. Therefore, for each synthesis method, it is necessary to understand and control key synthesis parameters such as pH, temperature, pressure, and metal-to-ligand molar ratio, in order to optimize the desired MOF structure for a target application.

The variation of the metal-to-ligand molar ratio in a MOF synthesis has been shown to affect the topology and dimensionality of the crystal structures. Wu et al.[52] reported the synthesis of $[\mathbf{Zn(hfipbb)(H_2hfipbb)_{0,5}}]_n$, a three-dimensional (3D) twofold parallel interpenetrating pillared network, and $[Zn_2(hfipbb)_2(dps)(H_2O)]_n$, a 3D bimodal-connected network with and without interpenetration, by varying the molar ratio M/L1/L2, where M = Zn, L1 = H_2hfipbb [H_2hfipbb = 4,4(hexafluoroisopropylidene)bis(benzoicacid)], and L2 = dps [dps = 4,4′-dipyridylsulfide]. Similarly, Liu et al.[53] studied the effect of varying the metal-to-ligand molar ratio M/L with M = Co and L = btze [btze = 1,2-bis(tetrazol-1-yl)ethane], obtaining the two-dimensional (2D) MOF $[\mathbf{Co(btze)_2(SCN)_2}]_n$ as well as one-dimensional (1D) linear chain $[\mathbf{Co(btze)_3(SCN)_2}]_n$ for molar ratios 1:1 and 1:2,

Received: January 25, 2019
Accepted: April 10, 2019
Published: April 24, 2019

DOI: 10.1021/acsomega.9b00236
ACS Omega 2019, 4, 7411−7419

respectively. Yuan et al.[54] showed the activation of different crystal growth patterns at a fixed molar ratio in M/L1/L2 mixtures by varying the reaction pH. Higher pH values favored the formation of the 3D interpenetrating framework $[\mathbf{Cd_2(CTPY)_4}]_n\cdot\mathbf{2H_2O}$, whereas lower pH values facilitate the formation of the 3D MOF $[Cd_2(CTPY)_2(ox)]_n$ without interpenetration.

Our work focuses on the synthesis of noncentrosymmetric MOFs with tetrazole-based ligands for which nonlinear optical activity is reported in powder form, for which phase matching is not possible.[55] Nonlinear optical MOF crystals could be used for applications in quantum cryptography based on entangled photon generation via spontaneous parametric down conversion, a second-order nonlinear quantum optical process, provided that phase-matching conditions can be achieved. Tetrazole compounds are promising ligands for the formation of nonlinear optical MOFs because of their strong dipolar characteristics[56] and large optical response.[57] From the synthetic point of view, tetrazole-based ligands are interesting because they possess a large number of coordination modes that can be selectively activated by varying the reaction pH, as recently demonstrated in ref 58 for the noncentrosymmetric MOF bis[5-(3-pyridyl)tetrazolato]zinc(II) $\mathbf{Zn(3\text{-}ptz)_2}$. This MOF crystal was first obtained by Wang et al.[59] using the Demko−Sharpless method for in situ formation of ligand 3-ptz starting from sodium azide (NaN_3) and 3-cyanopyridine in the presence of a suitable Lewis acid, giving $[\mathbf{Zn(3\text{-}ptz)_2}]$ under hydrothermal conditions for 24 h at 105 °C, using $ZnCl_2$ as the Lewis acid catalyzer. The Zn atom coordinates in a tetragonal type geometry, specifically in positions 1 and 4 of the tetrazole ring. This tetragonal geometry allows to generate a diamondoid-like 3D network. The 3-ptz ligand is formed in the manner proposed by Sharpless through to [2 + 3] cycloaddition. It is also interesting to note that $[\mathbf{Zn(3\text{-}ptz)_2}]$ crystallizes in an acentric space group $I\bar{4}2d$. Preliminary experimental results show that $\mathbf{Zn(3\text{-}ptz)_2}$ displays a moderate powder second-harmonic generation (SHG) response, ca. 0.4 times that of urea, allowing its applicability as a material for quantum communication. This feature is also similar to that of potassium dihydrogen phosphate (KDP) with a diamond-like network. We also produce the noncentrosymmetric MOF catena-($(\mu_3$-5-(3-pyridyl)tetrazol-*N*,*N*′,*N*″)-(μ_2-hydroxo)-zinc) $[\mathbf{Zn(OH)(3\text{-}ptz)}]$, obtained previously under different conditions.[60] The Zn atom has a five-coordinate geometry: in the equatorial plane, it is coordinated with three ligands 3-ptz, of which 1 comes from the pyridyl ring and the others come from positions 2 and 3 of the tetrazole ring, and in the axial position, it is coordinated to two hydroxyl bridging ligands, which gives the 2D character by repeating the −OH−Zn−OH−Zn−OH− chain in space. The adoption of acentric space groups *Fdd*2 $\mathbf{Zn(OH)(3\text{-}ptz)}$ prompted an investigation of their optical activity. Preliminary investigations show that SHG is active in the material. The zinc tetra-aquo coordination compound $\mathbf{Zn(H_2O)_4(3\text{-}ptz)_2}$[59] is also obtained as a byproduct. Besides, we report an alternative synthesis route for the nonporous 3D framework $[\mathbf{Zn(3\text{-}ptz)N_3}]$, which exhibits energetic behavior because of the presence of structural azide groups in the unit cell.[61] In Figure 1, we plot the set of pH and metal-to-ligand molar ratios used in this and previous work.

In this work, we study the effect of varying the molar ratio of the metal salt $Zn(NO_3)_2$ and the ligand precursor 3-cyanopyridine on the growth of noncentrosymmetric MOF structures and other compounds obtained. Keeping constant the molar ratios at which pure MOF crystals are obtained, we also studied the variation of the mixing pH and corresponding structures. We summarize the reaction parameter space explored in this work in Figure 1. The use of zinc nitrate results in overall better crystals of $[\mathbf{Zn(3\text{-}ptz)_2}]$ and $[\mathbf{Zn(OH)(3\text{-}ptz)}]$, for a given pH and molar ratio, in comparison with the synthesis involving zinc chloride.[59]

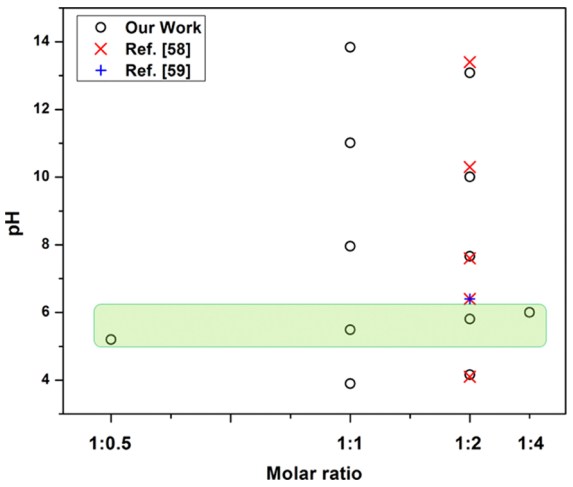

Figure 1. Reaction parameter space explored in this work starting from zinc nitrate (squares). Previous results based on zinc chloride from refs 58 and refs 59 are also shown. The shaded region corresponds to experiments done without any active pH control.

RESULTS AND DISCUSSION

We first searched for an optimal metal-to-ligand molar ratio to obtain high-quality $[\mathbf{Zn(3\text{-}ptz)_2}]$ crystals by keeping the pH unaltered relative to previous work in refs 58 and refs 59. For the metal-to-ligand molar ratios 1:1 and 1:2, we varied the pH to search for improved crystal quality in terms of purity, yield, and optical transparency. Figure 1 shows a decrease in pH as the amount of $Zn(NO_3)_2$ increases in the solution. This is due to the dissociation of the zinc salt into the Zn^{2+} cation solvated by water molecules (eq 1)

$$Zn(NO_3)_{2(s)} \xrightarrow{H_2O} Zn^{2+}{}_{(ac)} + NO_3^-{}_{(ac)} \quad (1)$$

$$Zn(H_2O)_6^{2+}{}_{(ac)} + H_2O \rightleftharpoons Zn(H_2O)_6(OH)^-{}_{(ac)} + H_3O^+{}_{(ac)} \quad (2)$$

As transition metals behave like Lewis acids, the Zn^{2+} hexahydrate complex, (pK_a = 9)[62] being the H_3O^+ ion is responsible for decrement in pH (eq 2). Increasing concentration of Zn^{2+} results into a greater number of H_3O^+, which means more acidic environment and hence lower pH of the solution.

Figure 2 shows the optical images of the products as obtained at different metal-to-ligand molar ratios such as 1:4, 1:2, 1:1, and 1:0.5, and further cool down to room temperature inside the furnace upon completion of the reaction time (24 h). In the stoichiometric ratio of 1:2, the pH was not controlled externally. The target compound is obtained at all molar ratios, but the metal-to-ligand ratio of 1:0.5 favors the high purity and maximum growth of the crystals. The byproducts obtained corresponding to each molar ratio are analyzed and summarized in Table 1. The pH reported are the pH measured

DOI: 10.1021/acsomega.9b00236
ACS Omega 2019, 4, 7411−7419

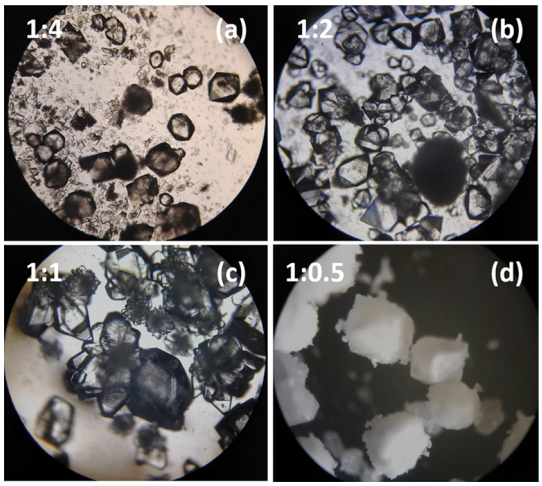

Figure 2. Optical images of the as-synthesized products at different metal-to-ligand molar ratios of 1:4 (a), 1:2 (b), 1:1 (c), and 1:0.5 (d).

Table 1. Main Product and Byproduct Obtained at Room Temperature for Different Metal-to-Ligand Molar Ratios without pH Control

molar ratio	mixing pH	product	byproduct
1:4	6.00	$Zn(3\text{-ptz})_2$	$Zn(H_2O)_4(3\text{-ptz})_2$
1:2	5.81	$Zn(3\text{-ptz})_2$	3-cyanopyridine
1:1	5.49	$Zn(3\text{-ptz})_2$	$Zn(3\text{-ptz})N_3$
1:0.5	5.20	$Zn(3\text{-ptz})N_3$	

immediately after mixing the reactants without any additional steps of pH control. The corresponding optical images and powder X-ray diffraction (XRD) patterns for each entry in Table 1 are shown in Figures 2 and 3, respectively.

For the molar ratio 1:4, we obtain that our target compound $Zn(3\text{-ptz})_2$ as well as the zinc tetra aquo complex $Zn(H_2O)_4(3\text{-ptz})_2$ (**ZAC**), which is relatively in large amount. The same products were obtained previously in ref 58 using

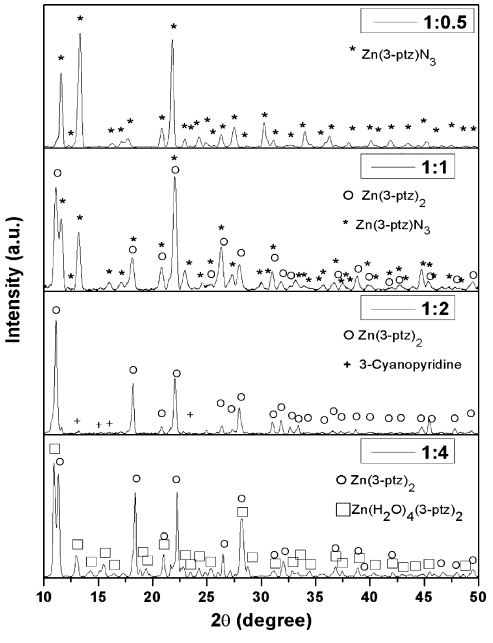

Figure 3. Powder XRD patterns for the products listed in Table 1.

half the amount of ligand. At the stoichiometric ratio of 1:2, we obtain $Zn(3\text{-ptz})_2$ along with very small quantity of non-reacted 3-cyanopyridine. As compared to ref 58, where at the same ratio (1:2) cocrystallization of **ZAC** and $Zn(3\text{-ptz})_2$ was obtained without any pH control. The difference in results in spite of having the same reaction time, temperature and pressure can only be attributed to the use of zinc nitrate (this work) salt instead of zinc chloride.[58] In general, we obtain $Zn(3\text{-ptz})_2$ crystals with improved size and better transparency with zinc nitrate than zinc chloride salt.

As we decrease the metal-to-ligand ratio below 1:2, we obtain increasing amounts of the recently reported energetic MOF $Zn(3\text{-ptz})N_3$ (μ-*N*)2-azido-[5-(3-pyridyl)tetrazolato]-zinc(II), a nonporous MOF with eight azide groups per unit cell.[61] It is worth to mention that this energetic MOF does not exhibit explosive behavior at the conditions used for its synthesis, filtration, and its spectroscopic characterization. For the molar ratio 1:1, we obtain $Zn(3\text{-ptz})N_3$ along with our target compound, whereas decreasing the amount of ligand to the molar ratio 1:0.5 gives only $Zn(3\text{-ptz})N_3$ in high yield and high purity, which represents an alternative synthesis route in comparison with ref 61.

The powder XRD patterns in Figure 3 show that our target MOF $Zn(3\text{-ptz})_2$ is present for metal-to-ligand molar ratios 1:4, 1:2, and 1:1. As expected, the stoichiometric ratio 1:2 gives a $Zn(3\text{-ptz})_2$ crystal phase with higher purity. Residual peaks correspond to unreacted 3-cyanopyridine. Increasing the relative abundance of the ligand relative to the stoichiometric ratio results in the formation of the aquo complex $Zn(H_2O)_4(3\text{-ptz})_2$ along with $Zn(3\text{-ptz})_2$. On the other hand, decreasing the relative abundance of the ligand relative to the stoichiometric ratio enhances the growth of $Zn(3\text{-ptz})N_3$. For the molar ratio 1:1, $Zn(3\text{-ptz})N_3$ is a minority product. For the molar ratio 1:0.5, the compound $Zn(3\text{-ptz})N_3$ (stoichiometric ratio 1:1) is the main reaction product. For such a high molar ratio, there is no sufficient availability of 3-ptz ligands to form our target MOF.

Figure 4 shows the scanning electron microscopy (SEM) images for the samples listed in Table 1. Figure 4b clearly

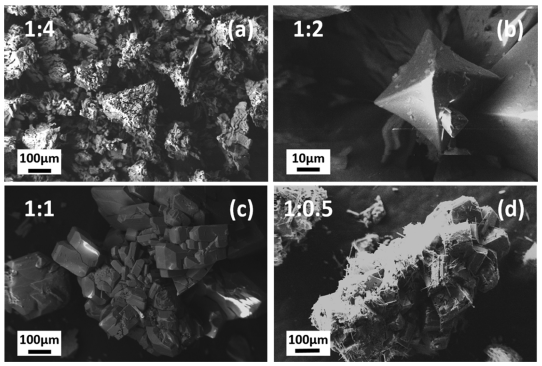

Figure 4. SEM images for the as-synthesized products at different metal-to-ligand molar ratios 1:4 (a), 1:2 (b), 1:1 (c), and 1:0.5 (d).

shows the octahedron morphology of the $Zn(3\text{-ptz})_2$ crystals formed. Crystal sizes obtained for $Zn(3\text{-ptz})_2$ in all experiments vary in the range 100−300 μm, which are typical sizes for reactions without pH control; all other reaction parameters are the same as in refs 58 and refs 59. For the stoichiometric metal-to-ligand ratio, the size of $Zn(3\text{-ptz})_2$ crystals is in general larger than those obtained at other molar ratios. This

DOI: 10.1021/acsomega.9b00236
ACS Omega 2019, 4, 7411−7419

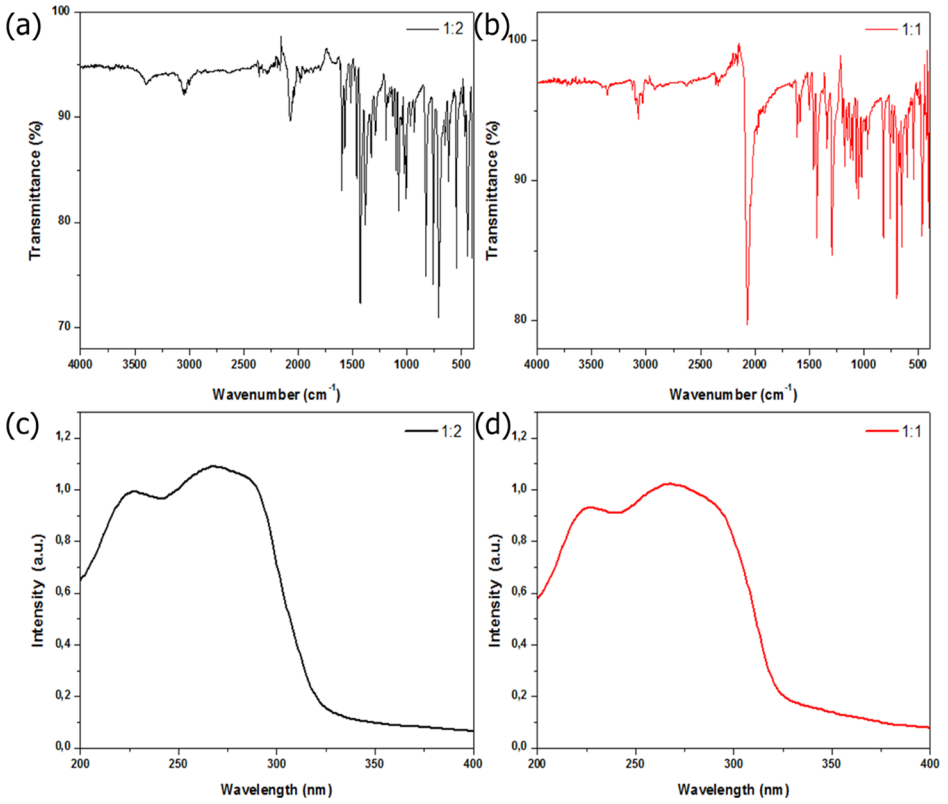

Figure 5. FTIR spectra of both samples obtained with metal-to-ligand molar ratios 1:2 (a) and 1:1 (b) without active pH control and solid-state UV−visible absorption spectra of both samples (c,d).

can be explained by the absence of competing nucleation events, leading to the growth of byproduct crystals, which also consume 3-ptz ligands. Figure 4a shows that the smaller byproduct crystals $\mathbf{Zn(H_2O)_4(3\text{-}ptz)_2}$ grow on the surface of $\mathbf{Zn(3\text{-}ptz)_2}$ crystals. The SEM images of the energetic MOF $\mathbf{Zn(3\text{-}ptz)N_3}$ crystals are shown in Figure 4c,d. The crystal size varies in the range 300−700 μm.

We also measured the Fourier transform infrared (FTIR) and solid-state UV−vis absorption spectra of the products listed in Table 1. The characteristic peak for tetrazole is observed at ∼1500 cm^{-1} in all the samples. The broad OH band peak is also observed at 3250 cm^{-1} at the molar ratio 1:4, associated with the aquo complex $\mathbf{Zn(H_2O)_4(3\text{-}ptz)_2}$. Figure 5a shows that at the stoichiometric ratio 1:2, the FTIR spectrum exhibits a weak peak at 2073 cm^{-1}, which can be assigned to the −CN bond of unreacted 3-cyanopyridine. For the molar ratio 1:1, a strong and narrow peak is observed at 2070 cm^{-1}, which can be assigned to the azido group ($-N_3$) that forms the energetic MOF $\mathbf{Zn(3\text{-}ptz)N_3}$. The strong azido IR peak ($-N_3$) is also observed for repetitions for the synthesis at the molar ratio 1:0.5, for which $\mathbf{Zn(3\text{-}ptz)N_3}$ is the main product. The UV−visible absorption spectra show that in the both samples, there is no absorption in the visible range because the metal center Zn has a complete valence d^{10} orbital. The absorption of both samples are dominated by the $\pi-\pi^*$ transitions of the 3-ptz ligand.[58] In the sample metal−ligand ratio 1:2, three strong absorption peaks are seen at 227, 266, and 288 nm with very low intensity, whereas in the sample metal−ligand ratio 1:1, three absorption peaks are clearly visible at 227, 266, and 303 nm. The first two peaks correspond to the absorption peak of ligand 3-ptz as shown in the Supporting Information S4b and the peak at 288 nm of the sample 1:2 corresponds to the absorption band of 3-cyanopyridine as shown in Supporting Information S4c. The peak at 303 nm of the sample molar ratio 1:1 also corresponds to a peak of the ligand. This peak is more intense in this sample because both the product and the subproduct have the ligand 3-ptz in its structure, unlike the sample with a molar ratio 1:2.

Effect of Reaction pH at Fixed Molar Ratio. In addition to the variation of molar ratio, we explore the effect of changing the pH of the solution at the stage of mixing the reactants, whereas during the reaction in the furnace the pH is unmonitored. We vary the pH as described in ref 58 for two sets of experiments: one set for the molar ratio 1:2, which is the stoichiometric ratio of $\mathbf{Zn(3\text{-}ptz)_2}$, and another set for the molar ratio 1:1, which is the stoichiometric ratio of $\mathbf{Zn(3\text{-}ptz)N_3}$. The main products obtained in each set of experiments are summarized in Tables 2 and 3.

For the molar ratio 1:2 (Table 2), our results are qualitatively in agreement with those in ref 58. In general, increasing the mixing pH above the uncontrolled pH level (5.81) favors the formation of the 2D MOF $\mathbf{Zn(OH)(3\text{-}}$

Table 2. Products As Obtained at Different pH for the Metal-to-Ligand Molar Ratio 1:2[a]

pH	product	subproduct
4.67	$\mathbf{Zn(3\text{-}ptz)_2}$	3-cyanopyridine
*5.81	$\mathbf{Zn(3\text{-}ptz)_2}$	3-cyanopyridine
7.66	$\mathbf{Zn(OH)(3\text{-}ptz)}$	ZnO
10.01	$\mathbf{Zn(OH)(3\text{-}ptz)}$	ZnO
13.08	ZnO	

[a]The pH labeled with an asterisk coincides with Table 1.

DOI: 10.1021/acsomega.9b00236
ACS Omega 2019, 4, 7411−7419

Table 3. Products As Obtained at Different pH for the Metal-to-Ligand Molar Ratio 1:1[a]

pH	product	subproduct
3.90	**Zn(3-ptz)$_2$**	3-cyanopyridine
*5.49	**Zn(3-ptz)$_2$**	**Zn(3-ptz)N$_3$**
7.96	**Zn(OH)(3-ptz)**	ZnO
11.01	**Zn(OH)(3-ptz)**	ZnO
13.84	ZnO	

[a]The pH labeled with an asterisk coincides with Table 1.

ptz),[58,60] as the ions $Zn(OH)^+$ and $Zn(OH)^{2+}$ become the most abundant species (>99%) in the pH range 6−11 at 75 °C.[63] Near pH 13, we obtain an almost exclusive formation of zinc oxide (ZnO), in agreement with ref 58. Powder XRD and FTIR spectra confirmed it and these results are shown in the Supporting Information S1 and S3.

We obtain roughly the equal crystal yield and reaction products in the case of uncontrolled pH (5.81) and at pH = 4.67, controlled by nitric acid. The powder XRD spectra for both samples are indistinguishable (see the Supporting Information), both confirming the presence of **Zn(3-ptz)$_2$** and 3-cyanopyridine. The optical images in Figure 6 show that

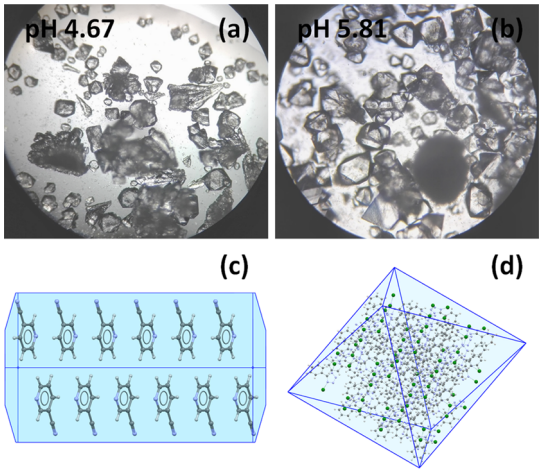

Figure 6. Optical images for samples in Table 2 at pH 4.67 (a) and pH 5.81 (b) for the metal-to-ligand molar ratio 1:2. The simulated crystal habits of 3-cyanopyridine (c) and **Zn(3-ptz)$_2$** (d) are also shown.

at pH 4.67, the **Zn(3-ptz)$_2$** octahedrons coexist with large number of 3-cyanopyridine molecular crystals, whose observed crystal habit is consistent with simulations. The more intense −CN peak in the IR spectrum shown in Figure 7a confirms the greater abundance of unreacted 3-cyanopyridine at lower pH in comparison with pH 5.81. Unreacted 3-cyanopyridine can result from the protonation of azide ions (N_3^-) at low pH. As the azide ion captures a proton, its availability to participate in the cycloaddition reaction that forms 3-ptz ligands[64] is significantly reduced.

Figure 8 shows the SEM images of the samples as listed in the Table 2. Figure 8a−d shows the **Zn(3-ptz)$_2$** MOF octahedrons obtained at the low pH, whose size varies in the range 100−300 μm. For alkaline environments (pH 7.77 and 10.01), we obtain the large rodlike structures characteristic of the MOF crystal **Zn(OH)(3-ptz)**, which has a 2D coordination framework.[58,60] At pH 10.01, we obtain large microrods

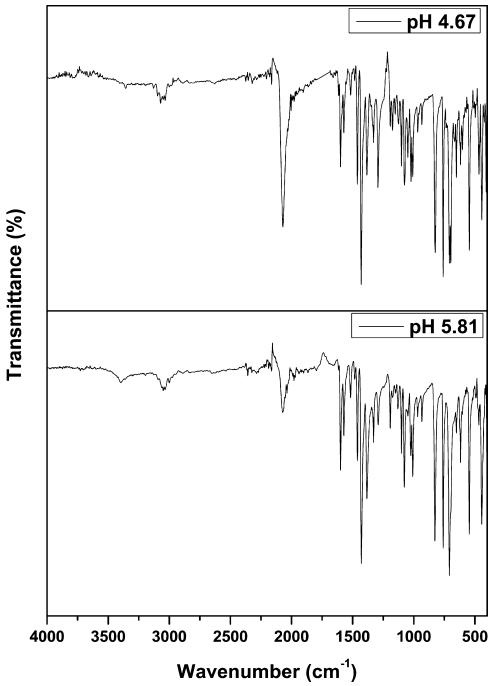

Figure 7. FTIR spectra of the samples at pH= 4.67 and 5.81 (Table 2) for the metal-to-ligand molar ratio 1:2.

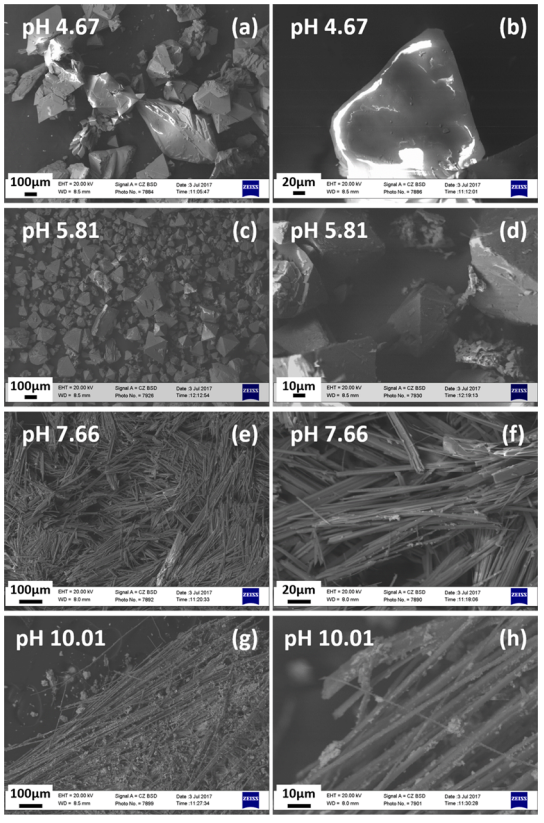

Figure 8. (a−h) SEM images of the as-obtained samples at different pH for the constant metal-to-ligand molar ratio of 1:2.

with lengths in the range 300 μm to 1.8 mm, which is 10^4 times higher than previously reported,[58,60] for the same reaction times and temperatures. The rod widths vary in the range 2−30 μm, which is up to 10 times higher as previous reports. We

DOI: 10.1021/acsomega.9b00236
ACS Omega 2019, 4, 7411−7419

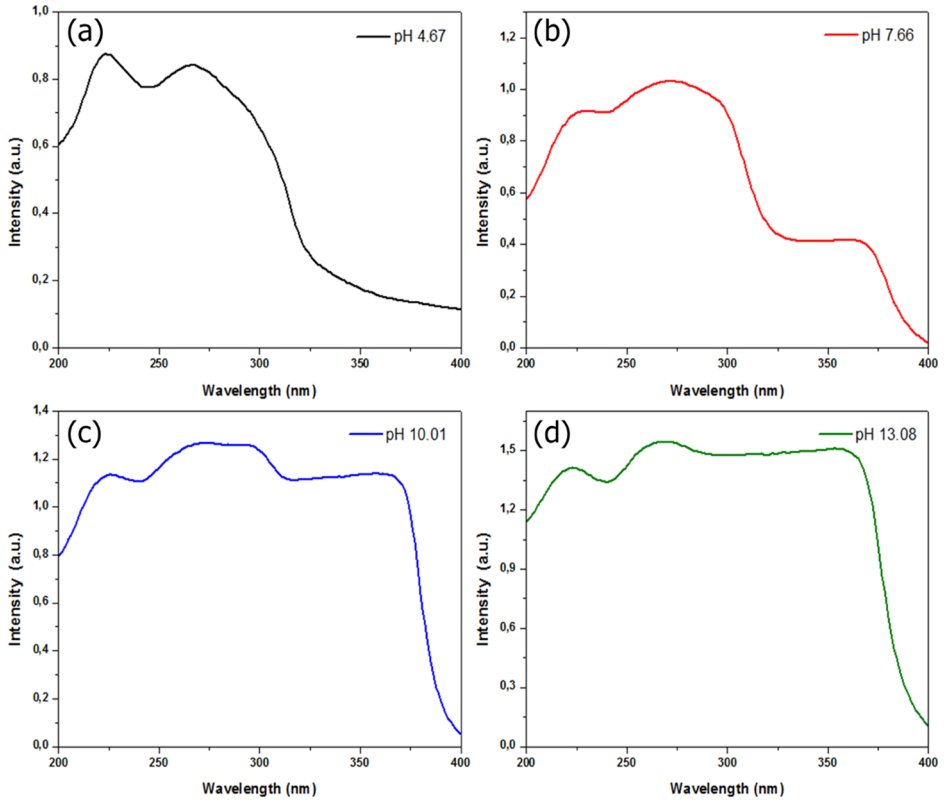

Figure 9. UV−vis solid spectra of the samples at different pH of 4.67 (a), 7.66 (b), 10.01 (c), and 13.08 (d) for the metal-to-ligand molar ratio 1:2.

attribute this improvement in size is due to the use of zinc nitrate instead of zinc chloride.[58,60]

Figure 9 shows UV−visible absorption spectra of the solid samples obtained at pH = 4.67, 7.66, 10.01, and 13.08. In all the samples, it can be seen that there is no absorption in the visible range because of the filled d^{10} orbital of the Zn metal centers. The sample at pH = 4.67 has the same absorption peaks as that of the sample at pH = 5.81 as shown in Figure 5c. Both have the same products and subproducts and hence, the absorption bands are given by the transitions occurring in the 3-ptz ligand. The absorption band of ZnO is observed in all three samples with basic pH, and their intensity increases as the pH increases because of the formation of a greater number of ZnO crystals. The absorption peaks of the ligand 3-ptz are also clearly observed in the sample at pH = 7.66 as shown in Figure 9b, whereas at higher pH, it is suppressed because of higher intensity of the ZnO peak (Figure 9c,d).

In a second set of experiments, we fixed the metal-to-ligand molar ratio to 1:1, which is the stoichiometric ratio for the energetic MOF **Zn(3-ptz)N_3**,[61] and varied the mixing pH as specified in Table 3. Figure 10 shows the optical images of the products as obtained at pH = 3.90 and 5.49. The corresponding powder XRD patterns are given in Figure 11a,b. Despite obtaining similar total crystal yields and target MOF **Zn(3-ptz)$_2$** for the both acidic conditions explored, the overall results are qualitatively different. While Figure 10b shows that without active pH control (pH = 5.49), a significant amount of **Zn(3-ptz)N_3** is formed in a mixed phase with **Zn(3-ptz)$_2$**, whereas at pH = 3.90 there are no traces of the energetic compound. We understand this in terms of a lower availability of azide ions N_3^- to form coordination bonds with zinc at lower pH. At the mixing temperature (25 °C), the relative abundance of azide ions in solution is less than 13% (pK_a = 4.72[65]). On the other hand, for pH 5.49, the relative abundance of azide ions is about 85%. Figure 10c shows that at pH = 7.96, we obtain predominantly **Zn(OH)(3-ptz)** and ZnO. Additional XRD data (as shown in Supporting Information S2) confirm that as the pH is increased beyond 8.0, the growth of ZnO is favored over **Zn(OH)(3-ptz)**.

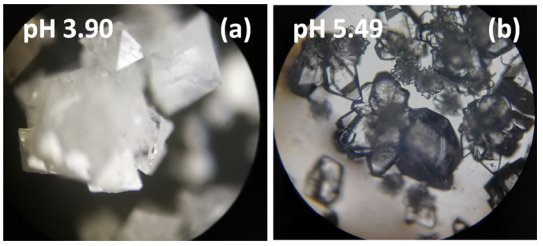

Figure 10. Optical images for samples in Table 3 at pH = 3.90 (a) and pH 5.49 (b) for the metal-to-ligand molar ratio 1:1.

CONCLUSIONS

We explored a set of hydrothermal synthesis parameters to optimize the growth of the transparent noncentrosymmetric MOFs [**Zn(3-ptz)$_2$**] and [**Zn(OH)(3-ptz)**], which have been proposed for applications in nonlinear optical signal processing with phase matching. By varying the metal-to-ligand molar ratio and the mixing pH, we find that high-quality [**Zn(3-ptz)$_2$**] can be obtained in large quantities at the molar ratios 1:2 and 1:1. For the molar ratio 1:2 and pH around 4.2, the [**Zn(3-ptz)$_2$**] crystals with improved transparency and purity are obtained. In alkaline environments (pH 7−10), we obtain large rodlike [**Zn(OH)(3-ptz)**] crystals with lengths approaching to the millimeter regime. This is a 4 order of magnitude improvement over previous reports. All samples were obtained

DOI: 10.1021/acsomega.9b00236
ACS Omega 2019, 4, 7411−7419

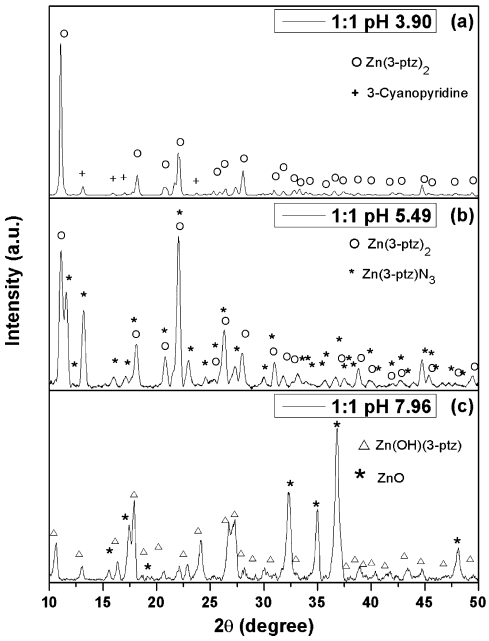

Figure 11. Powder XRD patterns of the products listed in Table 3 for pH = 3.90 (a), pH 5.49 (b), and pH 7.96 (c).

by using nitrate (NO_3^-) as a zinc counter ion, which is found to achieve better-quality crystals in comparison with previously used zinc chloride salts. In addition we found a simple alternative synthesis route for the growth of $[\mathbf{Zn(3\text{-}ptz)N_3}]$, a high-energy MOF that has been reported recently.[61]

The results obtained are promising for the development of MOF-based nonlinear optical devices. The high transparency and increasing size of the $[\mathbf{Zn(3\text{-}ptz)_2}]$ crystals obtained at lower mixing pH show the potential for further optimization of the reaction acidity. Reaching to single-crystal sizes in the millimeter regime would enable optical characterization such as Mueller polarimetry as well as SHG with phase matching. Moreover, the record lengths obtained for the $[\mathbf{Zn(OH)(3\text{-}ptz)}]$ crystals would facilitate the simple alignment of the rodlike structures on a substrate using mechanical stress. Such aligned quasi-1D crystals can be used as nonlinear waveguides for efficient generation of SHG signals using standard microscopy techniques. Nonlinear optical MOF waveguides would allow the development of alternative materials for scalable integrated quantum photonics.[66]

METHODS

The Zn-to-(3-ptz) molar ratio (metal-to-ligand) was varied by using 1, 2, 4, and 8 mmol of $Zn(NO)_3{\cdot}6H_2O$, keeping the amount of 3-cyanopyridine and NaN_3 fixed to 4 and 6 mmol, respectively. The corresponding molar ratios are 1:4, 1:2, 1:1, and 1:0.5. All reagents were mixed in a bottle with a screw cap, and 6 mL of distilled water was added at room temperature. For the set of experiments at fixed molar ratio of 1:2 and 1:1, the pH was fixed by using nitric acid at 70% (Sigma Aldrich) and KOH = 18.8 M. After measuring the pH of the solution, the samples were kept in an oven for 24 h at 105 °C. The samples were left for another 24 h inside the oven for cooling to room temperature. After cooling, the obtained samples were washed with ethanol and left for another 24 h to desiccate in vacuum. XRD analysis was done with a Shimadzu XRD 6000 diffractometer using Cu Kα (l = 1.5418 Å) radiation. Microstructural characterization of the synthesized materials was done by a scanning electron microscope Zeiss EVO MA10. pH was measured with a pH meter 2700 Oakton. FTIR measurements were taken with a JASCO FTIR-4600 spectrophotometer equipped with an ATR Pro ONE. UV–visible spectra of solid samples were recorded at room temperature by using a PerkinElmer Lambda 750 spectrophotometer.

ASSOCIATED CONTENT

Supporting Information

The Supporting Information is available free of charge on the ACS Publications website at DOI: 10.1021/acsomega.9b00236.

XRD spectra of the samples as obtained at pH = 4.67, 5.81, 7.66, 10.01, and 13.08 for the metal-to-ligand molar ratio of 1:2; XRD spectra of the samples at pH = 3.90, 5.49, 7.96, 11.01, and 13.84 for the metal-to-ligand molar ratio of 1:1; FTIR spectra of the samples at different pH of 3.90, 7.96, 11.01, and 13.84 for the metal-to-ligand molar ratio of 1:2; and UV–visible spectra of the sample at the molar ratio of 1:0.5, 3-cyanopyridine and the ligand 5-(3-pyridyl)-1*H*-tetrazole reagents (PDF)

AUTHOR INFORMATION

Corresponding Authors

*E-mail: felipe.herrera.u@usach.cl (F.H.).
*E-mail: dineshpsingh@gmail.com (D.P.S.).

ORCID

Javier Enríquez: 0000-0002-2502-5787
Felipe Herrera: 0000-0001-8121-1931
Dinesh Pratap Singh: 0000-0002-2893-7749

Notes

The authors declare no competing financial interest.

ACKNOWLEDGMENTS

We thank Gustavo Cañas for helpful suggestions. J.E. and D.P.S. are supported by Proyecto Basal USA 1799 VRIDEI and Fondecyt Regular 1151527. F.H. is supported by CONICYT through the Proyecto REDES ETAPA INICIAL, Convocatoria 2017 no. REDI 170423, and FONDECYT Regular No. 1181743. F.H. and D.P.S. also thank the support by Iniciativa Cientifica Milenio (ICM) through the Millennium Institute for Research in Optics (MIRO).

REFERENCES

(1) Yaghi, O. M.; Li, H. Hydrothermal Synthesis of a Metal-Organic Framework Containing Large Rectangular Channels. *J. Am. Chem. Soc.* **1995**, *117*, 10401–10402.
(2) Li, H.; Eddaoudi, M.; O'Keeffe, M.; Yaghi, O. M. Design and synthesis of an exceptionally stable and highly porous metal-organic framework. *Nature* **1999**, *402*, 276–279.
(3) Furukawa, H.; Yaghi, O. M. Storage of Hydrogen, Methane, and Carbon Dioxide in Highly Porous Covalent Organic Frameworks for Clean Energy Applications. *J. Am. Chem. Soc.* **2009**, *131*, 8875–8883.
(4) Farha, O. K.; Eryazici, I.; Jeong, N. C.; Hauser, B. G.; Wilmer, C. E.; Sarjeant, A. A.; Snurr, R. Q.; Nguyen, S. T.; Yazaydın, A. Ö.; Hupp, J. T. Metal-Organic Framework Materials with Ultrahigh Surface Areas: Is the Sky the Limit? *J. Am. Chem. Soc.* **2012**, *134*, 15016–15021.
(5) Deng, H.; Grunder, S.; Cordova, K. E.; Valente, C.; Furukawa, H.; Hmadeh, M.; Gandara, F.; Whalley, A. C.; Liu, Z.; Asahina, S.;

DOI: 10.1021/acsomega.9b00236
ACS Omega 2019, 4, 7411–7419

Kazumori, H.; O'Keeffe, M.; Terasaki, O.; Stoddart, J. F.; Yaghi, O. M. Large-Pore Apertures in a Series of Metal-Organic Frameworks. *Science* **2012**, *336*, 1018−1023.
(6) Farha, O. K.; Özgür Yazaydın, A.; Eryazici, I.; Malliakas, C. D.; Hauser, B. G.; Kanatzidis, M. G.; Nguyen, S. T.; Snurr, R. Q.; Hupp, J. T. De novo synthesis of a metal-organic framework material featuring ultrahigh surface area and gas storage capacities. *Nat. Chem.* **2010**, *2*, 944−948.
(7) Rosi, N. L.; Kim, J.; Eddaoudi, M.; Chen, B.; O'Keeffe, M.; Yaghi, O. M. Rod Packings and Metal−Organic Frameworks Constructed from Rod-Shaped Secondary Building Units. *J. Am. Chem. Soc.* **2005**, *127*, 1504−1518.
(8) Eddaoudi, M.; Kim, J.; Rosi, N.; Vodak, D.; Wachter, J.; O'Keeffe, M.; Yaghi, O. M. Systematic Design of Pore Size and Functionality in Isoreticular MOFs and Their Application in Methane Storage. *Science* **2002**, *295*, 469−472.
(9) Park, K. S.; Ni, Z.; Cote, A. P.; Choi, J. Y.; Huang, R.; Uribe-Romo, F. J.; Chae, H. K.; O'Keeffe, M.; Yaghi, O. M. Exceptional chemical and thermal stability of zeolitic imidazolate frameworks. *Proc. Natl. Acad. Sci. U.S.A.* **2006**, *103*, 10186−10191.
(10) Cavka, J. H.; Jakobsen, S.; Olsbye, U.; Guillou, N.; Lamberti, C.; Bordiga, S.; Lillerud, K. P. A New Zirconium Inorganic Building Brick Forming Metal Organic Frameworks with Exceptional Stability. *J. Am. Chem. Soc.* **2008**, *130*, 13850−13851.
(11) Kandiah, M.; Nilsen, M. H.; Usseglio, S.; Jakobsen, S.; Olsbye, U.; Tilset, M.; Larabi, C.; Quadrelli, E. A.; Bonino, F.; Lillerud, K. P. Synthesis and Stability of Tagged UiO-66 Zr-MOFs. *Chem. Mater.* **2010**, *22*, 6632−6640.
(12) Morris, W.; Volosskiy, B.; Demir, S.; Gándara, F.; McGrier, P. L.; Furukawa, H.; Cascio, D.; Stoddart, J. F.; Yaghi, O. M. Synthesis, Structure, and Metalation of Two New Highly Porous Zirconium Metal-Organic Frameworks. *Inorg. Chem.* **2012**, *51*, 6443−6445.
(13) Colombo, V.; Galli, S.; Choi, H. J.; Han, G. D.; Maspero, A.; Palmisano, G.; Masciocchi, N.; Long, J. R. High thermal and chemical stability in pyrazolate-bridged metal-organic frameworks with exposed metal sites. *Chem. Sci.* **2011**, *2*, 1311−1319.
(14) Lin, W.; Ma, L.; Evans, O. R. NLO-active zinc(ii) and cadmium(ii) coordination networks with 8-fold diamondoid structures. *Chem. Commun.* **2000**, 2263−2264.
(15) Du, F.; Zhang, H.; Tian, C.; Du, S. Synthesis and Structure of Two Acentric Heterometallic Inorganic-Organic Hybrid Frameworks with Both Nonlinear Optical and Ferroelectric Properties. *Cryst. Growth Des.* **2013**, *13*, 1736−1742.
(16) Ye, Q.; Li, Y.-H.; Song, Y.-M.; Huang, X.-F.; Xiong, R.-G.; Xue, Z. A Second-Order Nonlinear Optical Material Prepared through In Situ Hydrothermal Ligand Synthesis. *Inorg. Chem.* **2005**, *44*, 3618−3625.
(17) Ma, S.; Fillinger, J. A.; Ambrogio, M. W.; Zuo, J.-L.; Zhou, H.-C. Synthesis and characterizations of a magnesium metal-organic framework with a distorted (10,3)-a-net topology. *Inorg. Chem. Commun.* **2007**, *10*, 220−222.
(18) Liu, Y.; Li, G.; Li, X.; Cui, Y. Cation-Dependent Nonlinear Optical Behavior in an Octupolar 3D Anionic Metal-Organic Open Framework. *Angew. Chem., Int. Ed.* **2007**, *46*, 6301−6304.
(19) Lin, W.; Evans, O. R.; Xiong, R.-G.; Wang, Z. Supramolecular Engineering of Chiral and Acentric 2D Networks. Synthesis, Structures, and Second-Order Nonlinear Optical Properties of Bis(nicotinato)zinc and Bis{3-[2-(4-pyridyl)ethenyl]benzoato}-cadmium. *J. Am. Chem. Soc.* **1998**, *120*, 13272−13273.
(20) Evans, O. R.; Lin, W. Rational Design of Nonlinear Optical Materials Based on 2D Coordination Networks. *Chem. Mater.* **2001**, *13*, 3009−3017.
(21) Zhang, H.; Wang, X.; Teo, B. K. Molecular Design and Crystal Engineering of a New Series of Inorganic Polymers Separated by Organic Spacers: Structures of [(18C6)K][Cd(SCN)3] and [(18C6)-2Na2(H2O)2]1/2[Cd(SCN)3]. *J. Am. Chem. Soc.* **1996**, *118*, 11813−11821.
(22) Han, L.; Hong, M.; Wang, R.; Luo, J.; Lin, Z.; Yuan, D. A novel nonlinear optically active tubular coordination network based on two distinct homo-chiral helices. *Chem. Commun.* **2003**, 2580−2581.
(23) Wang, C.; Zhang, T.; Lin, W. Rational Synthesis of Noncentrosymmetric Metal-Organic Frameworks for Second-Order Nonlinear Optics. *Chem. Rev.* **2012**, *112*, 1084−1104.
(24) Rosi, N. L.; Eckert, J.; Eddaoudi, M.; Vodak, D. T.; Kim, J.; O'Keeffe, M.; Yaghi, O. M. Hydrogen Storage in Microporous Metal-Organic Frameworks. *Science* **2003**, *300*, 1127−1129.
(25) Férey, G.; Latroche, M.; Serre, C.; Millange, F.; Loiseau, T.; Percheron-Guégan, A. Hydrogen adsorption in the nanoporous metal-benzenedicarboxylate M(OH)(O2C-C6H4-CO2) (M = Al3+, Cr3+), MIL-53. *Chem. Commun.* **2003**, 2976−2977.
(26) Loiseau, T.; Serre, C.; Huguenard, C.; Fink, G.; Taulelle, F.; Henry, M.; Bataille, T.; Férey, G. A Rationale for the Large Breathing of the Porous Aluminum Terephthalate (MIL-53) Upon Hydration. *Chem.—Eur. J.* **2004**, *10*, 1373−1382.
(27) Chen, B.; Ockwig, N. W.; Millward, A. R.; Contreras, D. S.; Yaghi, O. M. High H2 Adsorption in a Microporous Metal-Organic Framework with Open Metal Sites. *Angew. Chem., Int. Ed.* **2005**, *44*, 4745−4749.
(28) Nagao, Y.; Ikeda, R.; Kanda, S.; Kubozono, Y.; Kitagawa, H. Complex-Plane Impedance Study on a Hydrogen-Doped Copper Coordination Polymer: N,N ′-bis-(2-hydroxyethyl)dithiooxamidato-copper(II). *Mol. Cryst. Liq. Cryst.* **2002**, *379*, 89−94.
(29) Shigematsu, A.; Yamada, T.; Kitagawa, H. Wide Control of Proton Conductivity in Porous Coordination Polymers. *J. Am. Chem. Soc.* **2011**, *133*, 2034−2036.
(30) Taylor, J. M.; Dawson, K. W.; Shimizu, G. K. H. A Water-Stable Metal-Organic Framework with Highly Acidic Pores for Proton-Conducting Applications. *J. Am. Chem. Soc.* **2013**, *135*, 1193−1196.
(31) Yamada, T.; Sadakiyo, M.; Kitagawa, H. High Proton Conductivity of One-Dimensional Ferrous Oxalate Dihydrate. *J. Am. Chem. Soc.* **2009**, *131*, 3144−3145.
(32) Xie, Z.; Ma, L.; deKrafft, K. E.; Jin, A.; Lin, W. Porous Phosphorescent Coordination Polymers for Oxygen Sensing. *J. Am. Chem. Soc.* **2010**, *132*, 922−923.
(33) Chen, B.; Wang, L.; Xiao, Y.; Fronczek, F. R.; Xue, M.; Cui, Y.; Qian, G. A Luminescent Metal-Organic Framework with Lewis Basic Pyridyl Sites for the Sensing of Metal Ions. *Angew. Chem., Int. Ed.* **2009**, *48*, 500−503.
(34) Lan, A.; Li, K.; Wu, H.; Olson, D. H.; Emge, T. J.; Ki, W.; Hong, M.; Li, J. A Luminescent Microporous Metal-Organic Framework for the Fast and Reversible Detection of High Explosives. *Angew. Chem., Int. Ed.* **2009**, *48*, 2334−2338.
(35) Della Rocca, J.; Lin, W. Nanoscale Metal-Organic Frameworks: Magnetic Resonance Imaging Contrast Agents and Beyond. *Eur. J. Inorg. Chem.* **2010**, 3725−3734.
(36) Liu, D.; Huxford, R. C.; Lin, W. Phosphorescent Nanoscale Coordination Polymers as Contrast Agents for Optical Imaging. *Angew. Chem., Int. Ed.* **2011**, *50*, 3696−3700.
(37) Lin, W.; Rieter, W. J.; Taylor, K. M. L. Modular Synthesis of Functional Nanoscale Coordination Polymers. *Angew. Chem., Int. Ed.* **2009**, *48*, 650−658.
(38) Rieter, W. J.; Pott, K. M.; Taylor, K. M. L.; Lin, W. Nanoscale Coordination Polymers for Platinum-Based Anticancer Drug Delivery. *J. Am. Chem. Soc.* **2008**, *130*, 11584−11585.
(39) Huxford, R. C.; Della Rocca, J.; Lin, W. Metal-organic frameworks as potential drug carriers. *Curr. Opin. Chem. Biol.* **2010**, *14*, 262−268.
(40) Bag, P. P.; Wang, X.-S.; Cao, R. Microwave-assisted large scale synthesis of lanthanide metal-organic frameworks (Ln-MOFs), having a preferred conformation and photoluminescence properties. *Dalton Trans.* **2015**, *44*, 11954−11962.
(41) Klinowski, J.; Almeida Paz, F. A.; Silva, P.; Rocha, J. Microwave-Assisted Synthesis of Metal-Organic Frameworks. *Dalton Trans.* **2011**, *40*, 321−330.
(42) Zou, R.-Q.; Jiang, L.; Senoh, H.; Takeichi, N.; Xu, Q. Rational assembly of a 3D metal-organic framework for gas adsorption with

DOI: 10.1021/acsomega.9b00236
ACS Omega 2019, 4, 7411−7419

predesigned cubic building blocks and 1D open channels. *Chem. Commun.* **2005**, 3526−3528.
(43) Li, P.; He, Y.; Guang, J.; Weng, L.; Zhao, J. C.-G.; Xiang, S.; Chen, B. A Homochiral Microporous Hydrogen-Bonded Organic Framework for Highly Enantioselective Separation of Secondary Alcohols. *J. Am. Chem. Soc.* **2014**, *136*, 547−549.
(44) Karizi, F. Z.; Safarifard, V.; Khani, S. K.; Morsali, A. Ultrasound-assisted synthesis of nano-structured 3D zinc(II) metal-organic polymer: Precursor for the fabrication of ZnO nano-structure. *Ultrason. Sonochem.* **2015**, *23*, 238−245.
(45) Mehrani, A.; Morsali, A.; Hanifehpour, Y.; Joo, S. W. Sonochemical temperature controlled synthesis of pellet-, laminate- and rice grain-like morphologies of a Cu(II) porous metal-organic framework nano-structures. *Ultrason. Sonochem.* **2014**, *21*, 1430−1434.
(46) Pilloni, M.; Padella, F.; Ennas, G.; Lai, S.; Bellusci, M.; Rombi, E.; Sini, F.; Pentimalli, M.; Delitala, C.; Scano, A.; Cabras, V.; Ferino, I. Liquid-assisted mechanochemical synthesis of an iron carboxylate Metal Organic Framework and its evaluation in diesel fuel desulfurization. *Microporous Mesoporous Mater.* **2015**, *213*, 14−21.
(47) Yan, D.; Gao, R.; Wei, M.; Li, S.; Lu, J.; Evans, D. G.; Duan, X. Mechanochemical synthesis of a fluorenone-based metal organic framework with polarized fluorescence: an experimental and computational study. *J. Mater. Chem. C* **2013**, *1*, 997−1004.
(48) Campagnol, N.; Souza, E. R.; De Vos, D. E.; Binnemans, K.; Fransaer, J. Luminescent terbium-containing metal-organic framework films: new approaches for the electrochemical synthesis and application as detectors for explosives. *Chem. Commun.* **2014**, *50*, 12545−12547.
(49) Martinez Joaristi, A.; Juan-Alcañiz, J.; Serra-Crespo, P.; Kapteijn, F.; Gascon, J. Electrochemical Synthesis of Some Archetypical Zn2+, Cu2+, and Al3+ Metal Organic Frameworks. *Cryst. Growth Des.* **2012**, *12*, 3489−3498.
(50) Bo, Q.-B.; Pang, J.-J.; Wang, H.-Y.; Fan, C.-H.; Zhang, Z.-W. Hydrothermal synthesis, characterization and photoluminescent properties of the microporous metal organic frameworks with 1,3-propanediaminetetraacetate ligand and its auxiliary ligand. *Inorg. Chim. Acta* **2015**, *428*, 170−175.
(51) Saha, D.; Maity, T.; Koner, S. Alkaline earth metal-based metal-organic framework: hydrothermal synthesis, X-ray structure and heterogeneously catalyzed Claisen-Schmidt reaction. *Dalton Trans.* **2014**, *43*, 13006−13017.
(52) Wu, Y.-P.; Li, D.-S.; Fu, F.; Dong, W.-W.; Zhao, J.; Zou, K.; Wang, Y.-Y. Stoichiometry of N-Donor Ligand Mediated Assembly in the ZnII-Hfipbb System: From a 2-Fold Interpenetrating Pillared-Network to Unique (3,4)-Connected Isomeric Nets. *Cryst. Growth Des.* **2011**, *11*, 3850−3857.
(53) Liu, P.-P.; Cheng, A.-L.; Yue, Q.; Liu, N.; Sun, W.-W.; Gao, E.-Q. Cobalt(II) Coordination Networks Dependent upon the Spacer Length of Flexible Bis(tetrazole) Ligands. *Cryst. Growth Des.* **2008**, *8*, 1668−1674.
(54) Yuan, F.; Xie, J.; Hu, H.-M.; Yuan, C.-M.; Xu, B.; Yang, M.-L.; Dong, F.-X.; Xue, G.-L. Effect of pH/metal ion on the structure of metal-organic frameworks based on novel bifunctionalized ligand 4′-carboxy-4,2′:6′,4″-terpyridine. *CrystEngComm* **2013**, *15*, 1460−1467.
(55) Boyd, R. W. *Nonlinear Optics*, 2nd ed.; Academic Press, 2003.
(56) Liu, D.-S.; Sui, Y.; Chen, W.-T.; Feng, P. Two New Nonlinear Optical and Ferroelectric Zn(II) Compounds Based on Nicotinic Acid and Tetrazole Derivative Ligands. *Cryst. Growth Des.* **2015**, *15*, 4020−4025.
(57) Zheng, Y.; Wang, S.-H.; Wu, S.-F.; Zheng, F.-K.; Wu, A.-Q. Tunable photoluminescence of a dual-emissive zinc(II) coordination polymer with an in-situ generated tetrazole derivative and benzenetetracarboxyli. *Inorg. Chem. Commun.* **2015**, *53*, 20−22.
(58) Chi-Durán, I.; Enríquez, J.; Manquian, C.; Wrighton-Araneda, K.; Cañon-Mancisidor, W.; Venegas-Yazigi, D.; Herrera, F.; Singh, D. P. pH-Controlled Assembly of 3D and 2D Zinc-Based Metal-Organic Frameworks with Tetrazole Ligands. *ACS Omega* **2018**, *3*, 801−807.
(59) Wang, L.-Z.; Qu, Z.-R.; Zhao, H.; Wang, X.-S.; Xiong, R.-G.; Xue, Z.-L. Isolation and Crystallographic Characterization of a Solid Precipitate/Intermediate in the Preparation of 5-Substituted 1H-Tetrazoles from Nitrile in Water. *Inorg. Chem.* **2003**, *42*, 3969−3971.
(60) Xiong, R.-G.; Xue, X.; Zhao, H.; You, X.-Z.; Abrahams, B. F.; Xue, Z. Novel, Acentric Metal-Organic Coordination Polymers from Hydrothermal Reactions Involving In Situ Ligand Synthesis. *Angew. Chem., Int. Ed.* **2002**, *41*, 3800−3803.
(61) Ignacio, C.-D.; Carolina, M.; Daniel, S.; Javier, E.; Felipe, H.; Dinesh Pratap, S. *Azide-Based High-Energy Metal-Organic Framework with Enhanced Thermal Stability*, 2018.
(62) Bertini, I.; Gray, H. B.; Lippard, S. J.; Valentine, J. S. *Bioinorganic Chemistry*; University Science Books, 1994.
(63) Reichle, R. A.; McCurdy, K. G.; Hepler, L. G. Zinc Hydroxide: Solubility Product and Hydroxy-complex Stability Constants from 12.5-75 °C. *Can. J. Chem.* **1975**, *53*, 3841−3845.
(64) Demko, Z. P.; Sharpless, K. B. Preparation of 5-Substituted 1H-Tetrazoles from Nitriles in Water†. *J. Org. Chem.* **2001**, *66*, 7945−7950.
(65) Patnaik, P. *Handbook of Inorganic Chemicals*; McGraw-Hill: New York, 2003; Vol. *529*.
(66) Moebius, M. G.; Herrera, F.; Griesse-Nascimento, S.; Reshef, O.; Evans, C. C.; Guerreschi, G. G.; Aspuru-Guzik, A.; Mazur, E. Efficient photon triplet generation in integrated nanophotonic waveguides. *Opt. Express* **2016**, *24*, 9932−9954.

DOI: 10.1021/acsomega.9b00236
ACS Omega 2019, 4, 7411−7419